Roadside Unit Visibility Prediction Method Based on SVR

Shaohong Ding, Yi Xu, Teng Sun, Jinxin Yu, Liming Wang, Ruoyu Zhu

***Abstract*— Visibility prediction in foggy conditions is a crucial aspect of intelligent driving. The conventional method for predicting visibility can forecast visibility, but it has poor resolution, lengthy programming time, and substantial error. This paper evaluates the visibility prediction and accuracy using image enhancement, dark channel-associated theory, and a deep convolutional neural model to address these issues. A deep learning model for visibility estimation derived from video data is established. First, the video is decomposed by MATLAB, and then the image is processed. The image is viewed as a two-layered discrete structure, and the slope capability is used to recover image sharpness estimates and determine image clarity. The quantitative value of clarity and visibility are trained. Finally, a trend of fog variation is predicted. The calculated meteorological optical reach (MOR) value is analyzed and adjusted to construct the MOR prediction function. Using support vector machine regression SVR, a period series forecast model is constructed. This model predicts that the future MOR value will predict the future fog variation trend and provide visual data for intelligent vehicles. This method effectively addresses the issue of inaccurate perceivability location goals and reduces the error margin of MOR, which can be used to determine the precise perceivability expectation of autonomous vehicles.**

***Index Terms*—Visibility prediction，Accuracy assessment，Dark channel prior method，SVR，Deep learning**

Manuscript received November 15, 2022; revised February 3, 2023.

This work was supported in part by the National Natural Science Foundation of China under Grant 51905320, Natural Science Foundation of Shandong Province under Grant ZR2022MF230 and ZR2021MG012, Shandong Province Major Science and Technology Innovation Project under Grant 2019JZZY010911, Shandong Key R&D Plan Project under Grant 2019GGX104066, Experiment technology upgrading project under Grant 2022003, and Shandong provincial programme of introducing and cultivating talents of discipline to universities: research and innovation team of intelligent connected vehicle technology.

Shaohong Ding is a postgraduate student at Shandong University of Technology, Zibo 255000, China. (e-mail: 1846336356@qq.com).

Yi Xu is an associate professor at the Collaborative Innovation Center of New Energy Automotive, Shandong University of Technology, Zibo 255000, China. (corresponding author, e-mail: xuyisdut@163.com).

Teng Sun is a postgraduate student at Shandong University of Technology, Zibo 255000, China. (e-mail: 877992783@qq.com).

Jinxin Yu is a postgraduate student at Shandong University of Technology, Zibo 255000, China. (e-mail: 2889717886@qq.com).

Liming Wang is a postgraduate student at Shandong University of Technology, Zibo 255000, China. (e-mail: 2463185675@qq.com).

Ruoyu Zhu is a postgraduate student at Shandong University of Technology, Zibo 255000, China. (e-mail: 1339315089@qq.com).

I. INTRODUCTION

Perceivability is, in many cases, communicated as an even distance, or as the place where the differentiation between a thing and the sky foundation rises to that of the natural eye's limit [1]. The longest horizontal distance at which a luminous point with a specific light intensity may be seen and found is known as the meteorological sight. Visibility is a key determinant of atmospheric transparency and air quality. In addition to the meteorological department, it is utilized in a variety of other industries, such as aviation, environmental monitoring, and others. For example, the steering by wire system [26] or man-machine driving steering torque [27,28] and speed control system [29] can be combined with the visibility prediction method to apply to vehicles running on the expressway to achieve safe driving under extreme conditions. The effectiveness and safety of urban transportation will be directly influenced by the accuracy of visibility forecasts. Zhou B. et al. [2] extended the NCEP short-range integrated prediction system with fog-integrated probability prediction. By simultaneously applying this technology to the description and evaluation of fog prediction and the same data for visibility analysis, the three models' ability to predict fog was significantly enhanced. Due to insufficient fog physics and limited model resolution, the fog prediction capability of some current models was insufficient to accurately predict the location and intensity of fog episodes. Sara Cornejo-Bueno S et al. [4] used the maximum likelihood approach and another technique known as the L-moment method to statistically analyze the optimal probability distribution for determining the duration of fog episodes. The elm method can produce extremely precise predictions of low-visibility events. Arun S H et al. [5] carried out 24-hour and 48-hour fog/visibility prediction for IGI airports. The fog-related meteorological parameters were derived from the IMDGFS model output, and the visibility was predicted and confirmed using METAR and weather observations. The prediction error of the method is small, but the performance of the 48-hour forecast requires improvement. Wagh S. et al. [22] studied the micro-physical structure of fog formed in a polluted environment and employed the fog index method to predict visibility.

Several studies predicted visibility using machine learning. Castillo-Botón C et al. [3] utilized a machine learning algorithm to solve the prediction problem in a dense fog and low visibility environment. Multi-layer perceptron provides the most accurate prediction results with an absolute error of approximately 350 m. Saadatseresht M [6] focused on the use of a counterfeit brain network in perceivability expectation and proposed another innovation in perceivability vulnerability forecasting based on the brain network. By training a multi-layer feed forward neural network, this technology can predict visibility. This strategy has the advantage of not requiring a re-initialization of the simulated brain network after adding images. Guijo-Rubio D et al. [7] proposed a hybrid prediction model that combines a fixed-size and a dynamic window and adjusts its size based on the dynamic changes of the time series. The real-time measurement of its data, however, reduces its operating time.

This paper proposes a depth learning model for visibility estimation based on video data as a solution to the issue of low operation efficiency. For the fog prediction performance of some existing models proposed by Zhou B et al. [2], due to the low model goal, the technique utilized in this paper is to obtain the picture sharpness data through the slope capability, to evaluate the picture clarity, and to train the depth learning model by quantifying the clarity and visibility, so as to improve its accuracy. Liaw J J et al. [8] proposed a perceptual haze thickness prediction model based on regular scene measurements and mist awareness factual qualities, which can predict the perceivability of haze scenes from an image without reference to the corresponding non-mist image. The AQI estimation model was developed using SVR to train the high-frequency data of ROI, RH and actual AQI. The visibility value was predicted by AOI. On this basis, this paper employs the SVR model to train the training data of known MOR value samples so as to enhance the accuracy of prediction. The primary commitments of this paper are as follows: 1) Through the foundation of perceivability and ground meteorological variables model, and the information is preprocessed; 2) A profound learning model for perceivability assessment in light of video information is laid out to evaluate the accuracy of the assessed perceivability; 3) The SVR model reflects the dynamic dependence of the data sequence and predicts the MOR value in the future.

This paper is organized as follows: Section 3 includes the foundation for the perceivability expectation model (Section 3.1) and the perceivability recognition calculation (Section 3.2). In Section 4, the video data obtained by the street estimation unit is processed, and the meteorological factors affecting visibility are analyzed to provide a foundation for the development of the deep learning model of visibility estimation. Section 5 compares the visibility value obtained by the visibility estimation deep learning model with the actual visibility value, verifies the model's feasibility, predicts the future visibility value over a period of time, and analyzes the significance of the visibility trend. Section 6 makes a final summary.

II. RELATED WORKS

As an essential aspect of automobile driving decisions, visibility forecasting has become an important area of study in recent years. Due to its simple operation, the monocular vision sensor has become the primary instrument for acquiring visibility data. To accelerate the process of obstacle recognition, many researchers have conducted relevant research. Conventional image object grouping and recognition calculations and systems struggle to meet the handling proficiency, execution, and knowledge requirements of images and videos with vast amounts of data. WanSik Won et al. [9] utilized low-cost sensors for coarse PM and fnePM; the moisture absorption characteristics of PM2.5; and the impact of the interaction between PM and fnePM and weather factors on visibility. The relationship between CPM and PM2.5 concentrations and weather observations was analyzed using a truncated regression model in order to infer the visibility value in this environment. Ashrit R [10] incorporated a real-time aerosol field into the high-resolution model to predict the airport's visibility. Examining the presentation of the coarse-goal worldwide model and the high-goal model for predicting provincial perceivability, and utilizing different statistical scores under very poor conditions (0-200 m), the accuracy of prediction in various visibility ranges was determined.

The visibility prediction model should have good prediction performance, accurate visibility prediction value, and high prediction efficiency. Sakaridis C. et al. [11] developed an improved RF model that provides more accurate visibility data and better prediction performance than the existing visualization models. Some researchers apply machine learning and deep learning to visibility prediction, which can effectively improve the accuracy of visibility prediction. By demonstrating a design similar to that of the human mind, profound gaining promotes the planning from low-level signs to undeniable level semantics to comprehend the progressive component articulation of information and has extraordinary visual data handling capabilities. Experiments conducted by Ren X et al. [12] have demonstrated that deep learning-based weather prediction is likely to become a supplement to conventional visibility prediction methods. DLWP is better than numerical weather prediction in terms of computability, comprehensiveness, Spatiotemporal scale, and interpretability. Yan S. et al. [13] proposed a perceivability forecast strategy based on blend calculation to improve perceivability expectation precision. Support vector machines, bit outrageous learning machines, irregular backwoods, and RBF brain networks are used to create the target capability of consolidated forecasting. The weighted coefficient of consolidated expectation estimation is advanced utilizing cuckoo search. The algorithm effectively increases the visibility's predictability. Zhang Y. et al. [14] proposed a method for visibility prediction based on six types of machine learning and the inversion layer's influencing factors. Using a weather process with poor visibility to compare numerical weather prediction and actual visibility, this method can enhance the ability to predict visibility. Han J H et al. [15] employed two distinct classification and regression methods, a model comprised of nine machine learning and three deep learning approaches, and three other techniques to identify and forecast the concentration of dense fog at sea.

Tao H C et al. [16] quantified photos based on data and videos in order to statistically assess the evolution trend of the fog. The sample data is preprocessed to eliminate any outlandish values, interpolate any missing locations, and conduct regression analysis on the image to create a regression model for the change in image visibility for visibility prediction. Tang P et al. [17] published an enhanced neural network deep learning approach as a mean square error visibility estimation algorithm for continuous surveillance video. The algorithm pulls an image from airport security footage every 15 seconds and selects a measuring area from each image's area of interest. The objective relapse capability of the mean square error layer of the Softmax layer convolutional brain network is replaced by the updated convolutional brain organization, and the angle drop method is utilized to fit the preparation to achieve continuous perceivability expectation. However, this method has low predictive accuracy. This study proposes a video-based deep learning model for visibility estimation to address the issue of low efficiency.

III. VISIBILITY PREDICTION METHOD BASED ON SVR

A laser visibility meter is a typical instrument for determining visibility. Currently, China's high-speed road network is gradually formed. Costs will be substantial if a large number of laser visibility meters are used to cover the national high-speed road network. In addition, laser visibility meters have deficiencies such as low mass fog detection accuracy, a limited detection range, and high maintenance costs. In recent years, the video-based road visibility detection method has gained popularity, which partially compensates for the shortcomings of the laser visibility meter. Image processing, artificial intelligence, and ambient optical analysis comprise the method for detecting video visibility. The relationship between video images and genuine circumstances is shaped by the examination and handling of video images, and the perceivability value is not fixed based on the change of picture highlights. The majority of this technique chooses a few films from which it extracts a few fixed and fixed characteristics [18,19]. The visibility accuracy of the estimates is limited because they are based on Koschmieder's rule and do not fully utilize continuous video information [20]. Because the formation and dissipation of fog have their own laws, it is usually related to the meteorological factors near the formation. First, the video data obtained by the road measurement unit are processed, and a suitable deep learning model for visibility prediction is established by measuring the ability gradient function [23-25]. Secondly, after filtering the image with the dark channel prior method, the video data are input into the visibility prediction model to calculate the video's visibility value. Finally, the visibility value for the subsequent time period is predicted based on SVR. Fig. 1 is the visibility prediction method process based on SVR.

The overall steps of the proposed method are as follows:

(1) At time t, the highway road measurement unit acquires a front view image as the target image for detecting visibility and performs gray processing. The region of interest is obtained through a cutting calculation, and the beginning and ending points of the path line within the region of interest are used as the corresponding highlight points. The relationship between the location of interest and the component points is established. The number of result and information hubs in the image is subdivided based on the confirmation requirements and the setting for the delivering effect, and the input node is recorded as $x(x=\{x_1,x_2,...,x_i\})$; the output node is denoted as $y(y=\{y_1,y_2,...,y_j\})$.

(2) At t, the monocular matching feature point C divides the camera's field of view into a matching area and a non-matching area, depending on whether the matching is successful. If the feature point C can be matched successfully, it belongs to the matching point, which is denoted as $Cx(Cx=\{Cx_1,Cx_2,...,Cx_i\})$. The region composed of matching points is the matching region; otherwise, it belongs to non-matching points, denoted as $Cd(Cd=\{Cd_1,Cd_2,...,Cd_n\})$.

(3) Morphological operations segment obstacles in unmatched regions. In view of the unclear or incomplete lane line in the image, the morphological activity is used to comprehend the endpoint extraction and path line alignment. Accepting that the pixel coordinate Dd of the confounded point Cd is (X_i,Y_j) $(i,j=1,2,...,n)$, the morphological shut activity is performed on the pixel coordinate Dd. Acceptably, the contact point between the path line and the street in the region of interest after two-layered morphological handling is denoted as $x(x=\{x_1,x_2,...,x_i\})$.

(4) The dark channel prior method is used to detect brightness difference visibility. The path line and street contact point obtained in step (3) are used as the information worth of the pixel point, the minimum value $J^c_{\min}(y)$ in the RGB channel is selected by screening, and the corresponding image is output. The $\Omega(x)$ region centered on each pixel in the image input pixel set $x(x=\{x_1,x_2,...,x_i\})$ is selected for minimal filtering. Since the transmittance $s(x)$ obtained by the dark channel prior method will have a fuzzy effect, it is necessary to introduce guide diagram I and the filtering output q to refine and distinguish the position relationship between the edge and the region. Assuming that the starting point of the lane line is d_1 and the ending point is d_2 , according to the national regulations, the length of the lane line is 6 meters, that is $d_1-d_2=6$, the atmospheric extinction coefficient β and the visibility estimation MOR can be calculated by the spacing and transmittance between the two points, and the accuracy of the visibility value is evaluated by Sobel and Roberts operators.

(5) For the results of accuracy evaluation in (4), if the accuracy is qualified, SVR visibility prediction is performed, and if the accuracy is not qualified, road pixels are reselected for accuracy evaluation, assuming that after accuracy evaluation, the MOR values that meet the accuracy are taken as an array, denoted as $(x_1,x_2,...,x_i)$; Select the prediction step size n and sample size i, set the MOR value of step size n after the prediction starts from $t-7$ moment, and incorporate the sample value $(x_{t-7},x_{t-6},...,x_t)$ into the model to calculate the MOR value y_1 at the next moment, Update the MOR array $(x_{t-7},x_{t-6},...,x_t)$ to $(x_{t-6},x_{t-5},...,x_t,y_1)$, and so on until the sample values in the MOR array are replaced by the predicted values, and record the MOR predicted value array $(y_1,y_2,...,y_n)$.

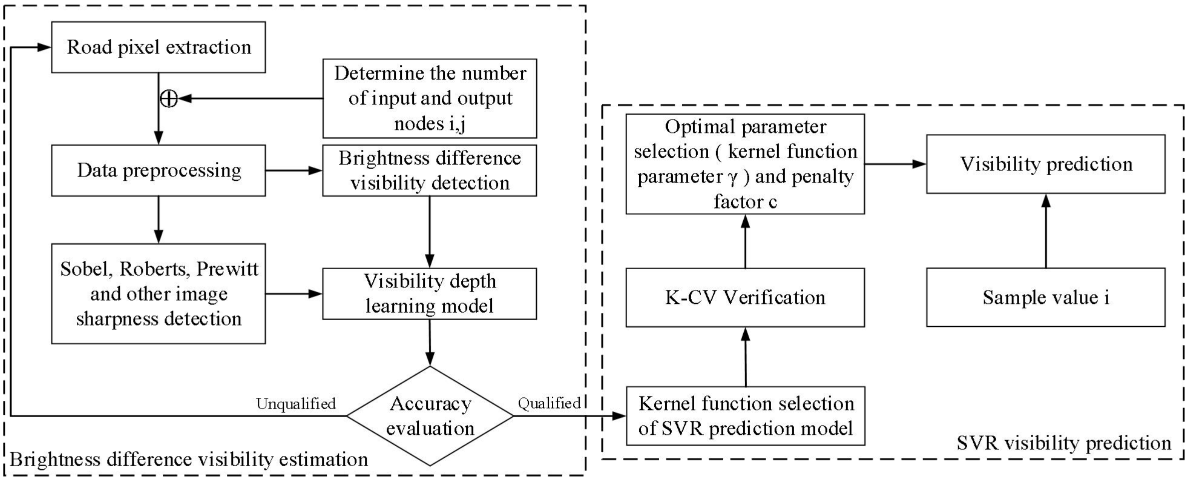

Fig. 1. Flow chart of the visibility prediction method based on SVR.

A. Measurement of the energy gradient function

To evaluate the accuracy of the predicted perceivability, we first develop a comprehensive learning model for perceivability assessment based on video information. We divide the video data captured by the visual sensor of the intelligent vehicle into frames to obtain more precise video data information, and then we select a period of time when the video was better lit. The second phase involves image processing. The image's dark data is obtained using the inclination capability, which views the image as a two-layered discrete lattice. The discrete sign's slope is addressed as a distinction. The deep learning model is trained by quantifying clarity and visibility. After image input, the video data processing method can calculate the image's clarity and output the corresponding visibility model.

Deep learning and conventional artificial neural networks differ substantially and share many similarities. Both use a multi-layer network with an input layer, a hidden layer, and an output layer, which is known as a hierarchical structure. Only the nodes in the adjacent layer are connected; those in the same layer or from different layers are not. Each layer can be viewed as a model of logical regression. In this paper, the idea behind the visibility prediction model is to preprocess an appropriate number of image frames and then treat the image as a two-dimensional discrete matrix during image processing. The gradient function is used to obtain information regarding image sharpness in order to evaluate image clarity. The quantified clarity value and visibility are used to train the deep learning model. The required images are then input into the model to calculate the clarity, and the model's accuracy is evaluated in comparison to the known data.

There is a greater slope value because the edge of the image in sharp focus is sharper and more distinct than the edge of the image in fuzzy defocus, and the dark value of the edge pixel varies significantly. Consequently, when an image is processed, it is regarded as a two-layered discrete grid, and the slope capability is used to assemble the image's dark data in order to assess the image's clarity. Energy slope capability EOG, Roberts capability, Tenengrad capability, Brenner capability, Variance capability, Laplace capability, and others are examples of normal inclination capabilities. This model employs the Energy of Gradient function, where the gradient value of each pixel is the sum of squares of the difference between the gray values of neighboring pixels in the x and y directions,

and the gradient value of all pixels is accumulated as the value of the clarity evaluation function. The expression is as follows:

$$F=\sum_{x}\sum_{y}\{[f(x+1,y)-f(x,y)]^2+[f(x,y+1)-f(x,y)]^2\} \quad (1)$$

B. Visibility calculation

1. Double luminance difference method

The twofold brightness qualification method, a suggested estimation based on the magnificence relationship method, can eliminate the influence of structure stray light and structure faint current on detectable quality area [11]. The double splendor distinction strategy for perceivability identification is presented, which is based on the approach of brightness correlation. The objective is to eliminate the influence of the CCD camera structure's faint current and establishment of stray light during the most popular method of recognizing detectable quality using the magnificence assessment procedure, and to construct the acknowledgment's exactness. The visibility detection formula for the twofold brightness difference approach is as follows:

$$V_d=\frac{3.912(L_2-L_1)}{\ln((G_{t1}-G_{g1})/(G_{t2}-G_{g2}))-\ln((B_{t1-0}-B_{g1-0})/(B_{t2-0}-B_{g2-0}))} \quad (2)$$

Among them, V_d represents the daytime meteorological visibility, L_i is the distance between the $i(i=1,2)$ target and the observation point $L_1<L_2$, G_{ti} and G_{gi} are the gray levels of the target and sky background measured by DPVS, respectively. B_{ti-0} and B_{gi-0} are the intrinsic brightness of the target and the brightness of the sky background that is consistent with the line of sight of the target observed from the location of the target, use dark target, $B_{ti-0}<B_{gi-0}$ and $G_{ti}<G_{gi}$.

There are still some issues with the double brightness method, such as the fact that when a vehicle is driving on a highway, there are typically trees and billboards near the road, which affect the gray information of the background sky.

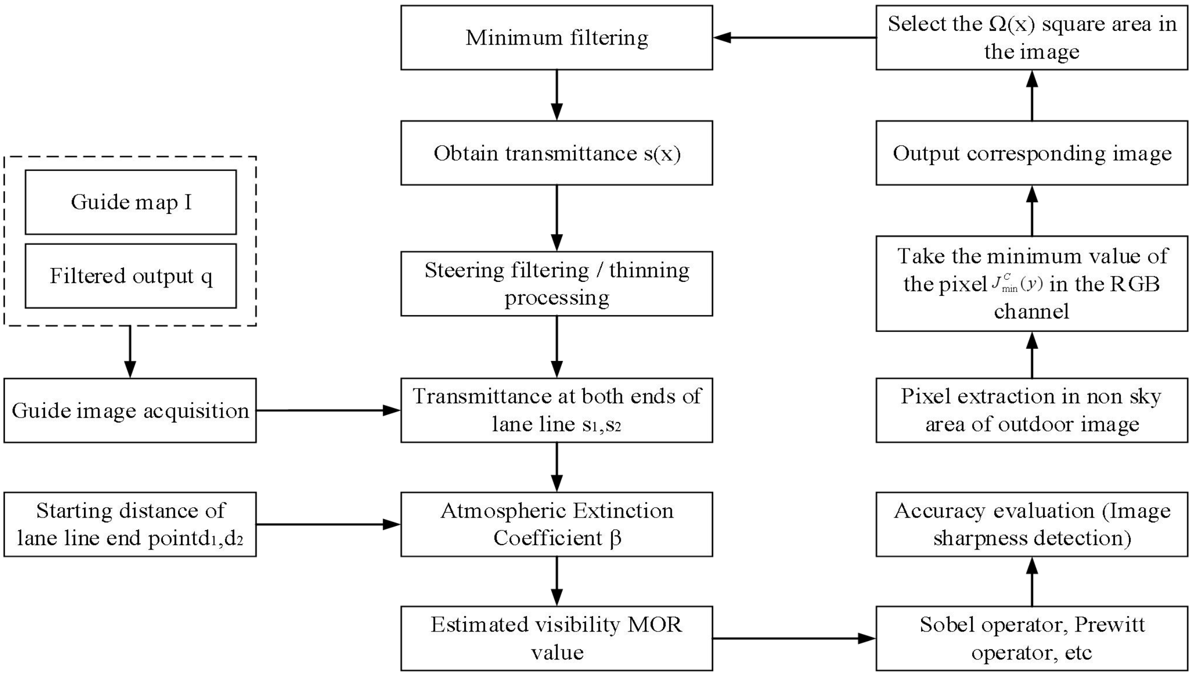

Fig. 2. Flow chart of visibility by the dark channel prior method.

Clearly, according to the video data, the humidity in the air is very high. The perceivability distinguished will have a significant error when the twofold brilliance differentiation strategy is subjected to climate conditions that result in the uneven transport of particles in the environment. Therefore, we employ another perceivability identification calculation: the dark channel prior method, which can significantly reduce the error in perceivability recognition caused by the uneven dispersion of particles in the atmosphere. The particular cycle is as figure 2 follow.

2. Visibility value based on lane line clarity detection

Due to the fact that the road video data obtained by the visual sensor contains time information, noise, and other interference information, the detection area of the video frame intercept is matted in MATLAB, and the matted image serves as the ROI area for the subsequent processing steps. The visibility value is then determined by the clarity of the detected lane lines in a fog environment.

He Kaiming summarized the previous information on a dim channel based on the trial analysis of a vast number of images, i.e., pixels in the non-sky region of outdoor images typically have at least one variety channel with a luminance value that is close to or equal to zero. This channel is known as the dark channel. The formula is:

$$J^{dark}(x) = \min_{c\in\{R,G,B\}} (\min_{y\in\Omega(x)} J^c(y)) = 0 \qquad (3)$$

In the formula, J^c is a color channel in the RGB three channels of the image, $\Omega(x)$ is a block area centered on x . J^{dark} is the dark channel, whose value is equal to or close to zero. The general procedure for calculating the image dark channel is to obtain the minimum value of each pixel RGB three channels in the image, outputting the image, and then filtering the minimum value of the image in the $\Omega(x)$ block area.

Then we need to obtain the transmittance to further calculate the visibility. Barometrical conveyance addresses the proportion of light force after optical way engendering to occurrence light power, which can be communicated as follows:

$$s(x) = 1 - \min_c(\min_{y\in\Omega(x)}(\frac{I^c(y)}{A^c})) \qquad (4)$$

Because there are many impurities in the image, we introduce a constant for correction. Then, we have:

$$s(x) = 1 - \omega\min_c(\min_{y\in\Omega(x)}(\frac{I^c(y)}{A^c})) \qquad (5)$$

Here, the constant is 0.95. In order to refine the conveyance determined by the aforementioned developments, a directed channel will be required. In the calculation system, the directed channel requires a directed image to channel. Permit channel manual to be a local direct model of guide diagram I and channel yield q. There is a direct connection between the directed image and q, which is established because we believe that the information provided by the directed image is primarily used to determine the location of the edge and the region. Therefore, during sifting, if the directed image indicates that the location is a district, it will be smoothed. If the guide is an edge, then hold onto these edge data. We mark the beginning stage organizes and the closure point directions of the path line, and work out the conveyance of the two endpoints as per their endpoint facilitates, which are signified as s_1 and s_2 . The atmospheric extinction coefficient β is then calculated. Firstly, we assume that the extinction coefficient is s , and the transmittance and depth of the scene are d . According to Koschmieder's theorem, the relationship between the three can be expressed as follows:

$$s = \exp^{-\beta d} \qquad (6)$$

The transmittance s_1 and s_2 of the starting point and the end point of one lane line in the image are obtained. Assuming that the starting distance is d_1 and the end distance is d_2 , the following formula can be obtained:

$$s_1 = \exp^{-\beta d_1} \qquad (7)$$

$$s_2 = \exp^{-\beta d_2} \qquad (8)$$

By dividing the (7) and (8) formulas, we have:

$$\beta = \frac{\ln \frac{s_1}{s_2}}{d_1 - d_2} \tag{9}$$

Because in the national standard, the highway lane length interval is consistent (6 meters), so we can know $d_1 - d_2 = 6$. Now we obtain the atmospheric extinction coefficient, according to the visibility formula:

$$MOR = \frac{\log(F/F_0)}{-\sigma} = \frac{\log(0.05)}{-\sigma} \tag{10}$$

C. PREDICTION OF MOR VALUE BASED ON SVR

According to known conditions, quantitative prediction of the MOR value calculated by 3.2.2 requires time series analysis of data. On the basis of the known limited visibility MOR observation data, a mathematical model based on SVR is developed to accurately reflect the dynamic dependence relationship contained in the sequence, and the future trend of fog is predicted. The change rule of visibility in the future period is determined, and the future MOR value is predicted. The specific procedure is depicted in Fig. 3.

1. Support vector regression

In order to establish a regression prediction model of MOR value on foggy days, the regression support vector machine is utilized in this paper. For known sample data MOR values, train the model using sample data containing MOR values. On the off chance that a bunch of information is examined as a preparation model, the example informational collection is (x_i, y_i), $i = 1, 2, .., n$. Among them, x_i represents the info section vector of the principal preparing test. Expecting that the model has i input factors and j yield factors, then $x_i = [x_i^1, x_i^2, ..., x_i^n]^T$, y_i are the comparing yield factors (true value). The linear regression function $T(x)$ of the SVR fog visibility prediction model is:

$$T(x) = w\Phi(x) + b \tag{11}$$

where w represents the weight vector, $\Phi(x)$ is a nonlinear mapping function, b denotes the bias vector. At the same time, considering the linear inseparability of SVR, the relaxation variables δ_i, δ_i^* are introduced to optimize the expression of the SVR visibility model in fog:

$$\varphi(w, \delta_i, \delta_i^*) = \min \frac{1}{2}\|w\|^2 + c\sum_{i=1}^{l}(\delta_i + \delta_i^*) \tag{12}$$

where c represents the penalty factor, which characterizes the size of the sample penalty when the error of meteorological optical range obtained by model training is greater than ε. Fig. 4 is the structure of SVR.

The Lagrange function is introduced into formula (12), which is converted into dual form and solved. The optimal solution of formula (12) is $a = [a_1, a_2, ..., a_l]$, $a^* = [a_1^*, a_2^*, ..., a_l^*]$. Thus, the regression function is converted to:

$$\begin{aligned} T(x) &= w^*\Phi(x) + b^* = \sum_{i=1} (a_i - a_i^*)\Phi(x_i)\Phi(x) + b^* \\ &= \sum_{i=1}^{l} (a_i - a_i^*)K(x_i, x) \end{aligned} \tag{13}$$

In the SVR prediction model established in this paper, we still need to consider the influence of the type of kernel function $K(x_i, x)$ on the performance of the model, and one cannot dismiss the importance of the penalty factor. Consequently, portion capability is an essential component of the SVR calculation. The straight, polynomial, sigmoid, and outspread premise capabilities are commonly utilized portion capabilities. The commonly used Gaussian spiral premise capability, which is depicted below, is selected as the bit capability of SVM after a thorough analysis. GRBF may accomplish nonlinear planning and limit SVM complexity, and fewer boundaries of the actual capability can diminish SVM intricacy.

$$GRBF(x, x_i) = \exp\left(-\frac{(x - x_i)^2}{2\sigma^2}\right) \tag{14}$$

where x_i represents the center of the kernel function, σ is the width parameter of the function, which controls the radial range of the function. In practical applications, GRBF is often simplified as Formula (14), and parameter γ is defined as the parameter of the GRBF kernel function.

$$GRBF(x, x_i) = \exp^{-\gamma(x - xi)^2} \tag{15}$$

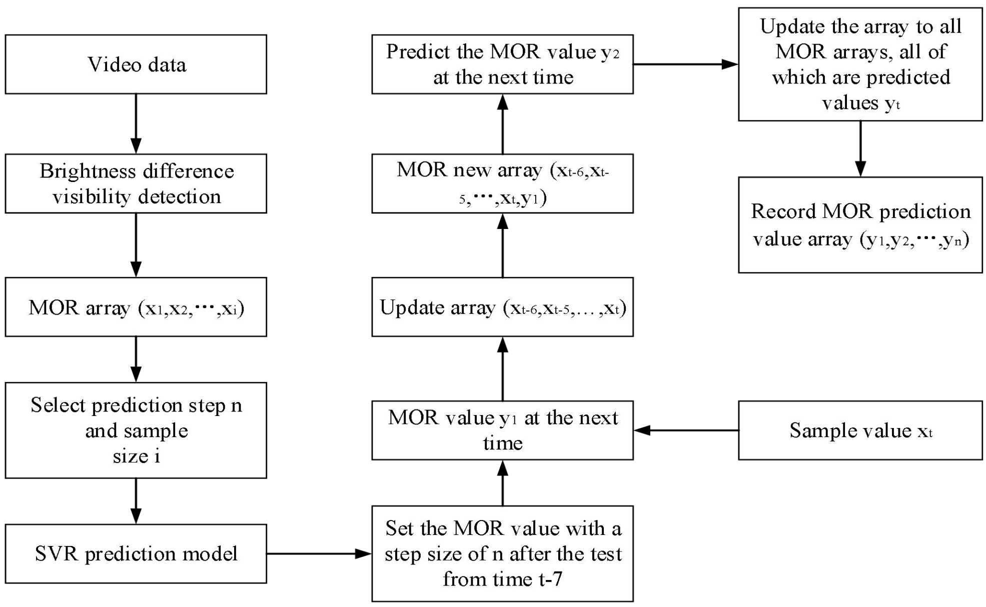

Fig. 3 The flow chart of the predicting MOR value based on SVR.

Kernel function parameter γ and penalty factor c in SVR model are usually obtained based on experience. However, some adjustments are needed to further improve the accuracy of model classification. Cross approval (K-crease Cross Validation, K-CV) can be utilized to choose the ideal boundaries to abstain from over-learning and under-learning.

CV arbitrarily divides the entire example set into k sections; one section is selected for each test set, and the other section, k-1, is used to generate the set that should be cycled k times. The classification accuracy of the model under the given parameters is represented by the mean value of classification accuracy in k cycles. The K-CV method can ensure that as many sample data as possible are included in model training, allowing the test results to ultimately reflect the classification performance of the model. In this paper, five-fold cross-validation (5-CV) is used to determine the model's accuracy. Fig. 5 depicts the precision of the SVM recognizable proof model with a step length of eight under a variety of part capability boundaries and punishment factor mixtures. If you wish to reduce over-identification, you can select the parameter combination with the smallest penalty factor.

Through (5-CV) confirmation, the most noteworthy exactness of the model is 0.93, and the SVM part capability boundary $\gamma = 1.84$ and the punishment calculate $c = 1.72$ models are set. In this paper, the K-overlay cross-approval strategy is shown to not only find the globally optimal arrangement, but also avoid the impact of ill-advised fitting, in order to improve the forecasting precision of the entire model. After constructing the SVR model, we must also construct a prediction function.

According to the change rule of the existing MOR data, we predict and analyze the MOR data and construct the time series prediction function as depicted (16):

$$y(t) = f(x(t-1), x(t-2), x(t-3), \ldots, x(t-n)) \tag{16}$$

Formulas (16) indicate that if we want to predict the MOR value at time t, we need the MOR value at the first n moments of time t as input to predict the MOR value at the current time t, where n is the step size.

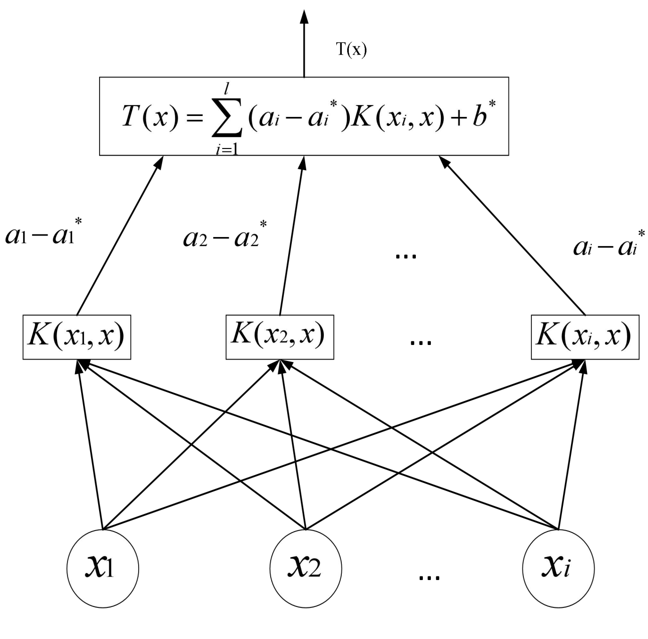

Fig. 4 SVR structure diagram.

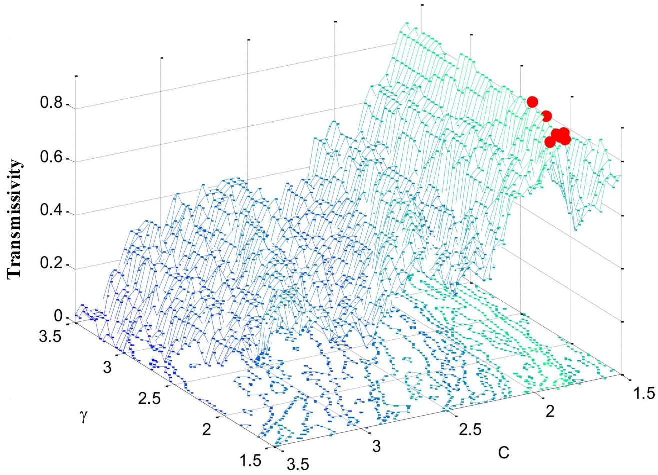

Fig. 5 Accuracy of the SVR identification model (note: red dots are the highest accuracy point in combination).

2. Specific steps for predicting future MOR values based on SVR

We can predict the MOR value for a period of time in the future based on the SVR model established in the preceding section. Using the principle of rolling prediction, meteorological optical sight data are predicted. The steps of rolling prediction principle are as follows:

Step 1: Input the existing MOR array $x_1, x_2, \ldots, x_t$ to SVR prediction model, get its prediction function until x_{t-7}.

Step 2: Starting from array $x_{t-7}, \ldots, x_t, y_1$, the next MOR value y_1 of x_t is predicted according to the SVR prediction model.

Step 3: Add y_1 to the end of the array, remove the original starting position x_{t-7} of the array, and input the new array $x_{t-7}, \ldots, x_t, y_1$ into the SVR prediction model, recursively predict the next MOR value y_2 of y_1.

Step 4: Repeat step 3 step by step to record all predicted values for predicted value $y_1, y_2, \ldots, y_n$.

IV. DATA PROCESSING

A. VIDEO PREPROCESSING AND DATA SELECTION

Firstly, the obtained video data must first be framed. Since the acquired video data from 0:1:40 to 0:36:56 central length is relatively stable, MATLAB is used to handle the video's casing in this range. The rate of casing is 25 edges/s, the underlying time is 26 seconds, and the casing number of the corresponding image at 0:1:40 is 1850 outline. The number of corresponding image frames is 54750. Video data sets generate 4 data per minute, averaging 15 seconds per data, so the data acquisition time for each minute is 10s, 25s, 40s, and 55s. From 0:02:00 to 0:37:00, 140 visibility points were collected. The images between [490,170] [490,580] [600,580] [600,170] were captured as the target images for energy gradient function measurement.

B. MOR DATA PREPROCESSING

To determine the relationship between visibility and ground meteorological observations (temperature, humidity, and wind speed), a model of visibility and ground meteorological factors must be developed. First, due to the fact that haze is related to ground meteorological variables, it is essential to explain the components of ground meteorological elements and to preprocess data such as ground meteorological variables. Secondly, according to the provided information, the model of perceivability and ground meteorological elements should be developed. Two types of visibility must be clarified here: RVR and MOR. RVR has a range of $(0,2000m]$ and MOR has a range of $(0,10000m]$. To evaluate the useful relationship between the two perceivability and the selected ground meteorological factors, it is necessary to select a number of ground meteorological components that exhibit a strong correlation with the two visibility. Finally, the linear relationship for real-time detection video data is produced, along with the functional relationship equation between visibility and climatic parameters.

1. Relevant data types

Meteorological factors include temperature, humidity, air pressure, wind speed, and other factors. Airport AMOS observation data provide meteorological factors and visibility information, as shown in Table 1.

2. Data preprocessing

Preprocessing generally refers to a series of cycles of handling and analyzing absent and unusual characteristics in the airport AMOS perception information and dimensionless information. Airport AMOS observation data may be missing and abnormal for a variety of reasons, including data acquisition equipment failure and storage data medium failure. These missing and abnormal values may affect the subsequent visibility analysis; therefore, they must be processed in advance. The pretreatment process is as follows:

1) Determination of missing and abnormal values in the data

The missing points in the original data can be determined by null value judgment. For the judgment of strange qualities, through the rule of 3δ, the recurrence in the gathered information test is not exactly the preset recurrence limit, that is, $p(|x-\mu|>3\delta=0.003)$, and the data with distribution proportion less than 1% are taken as abnormal values.

2) Treatment of missing values and abnormal values

Using Lagrange interpolation formula $L(x)=\sum_{a=0}^{n}\prod_{b=0,b\neq a}^{n}\frac{x-x_b}{x_a-x_b}ab$ at missing points and outliers, the approximate values at corresponding points of missing or outliers are obtained, where n represents the total number of line-of-sight data, x_a represents the first data, and x_b represents the second data.

3) Data noise reduction

Using EMD (Empirical Mode Decomposition) to find out the maximum and minimum values of all kinds of data are: $e_{\max(t)}$ and $e_{\min(t)}$. Calculate the mean value of the maximum and minimum $m(t)=(e_{\max(t)}+e_{\min(t)})/2$, and then extract the details $d(t)=x(t)-m(t)$. Repeat the above process until the mean value of $d(t)$ is 0, so as to achieve the purpose of data noise reduction.

3. Data trend, correlation analysis, and main index selection

The patterns of perceivability data, temperature data, mugginess data, and normal breeze speed were divided to focus on the progressions in perceivability and meteorological variables over the course of a day.

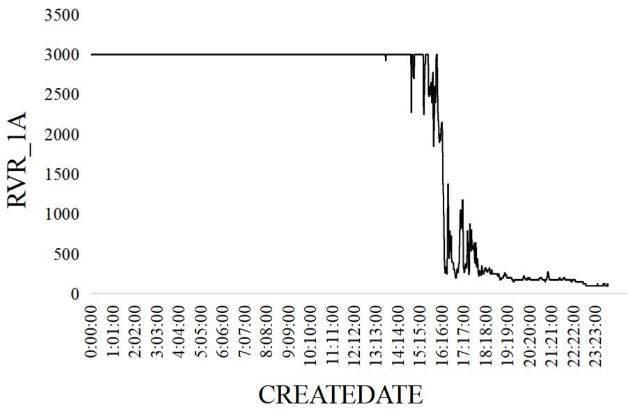

Fig. 6 RVR_1A relative time variation curve.

Between 0:00 and 14:50, the runway visual range (RVR) was basically maintained at 3000, between 14:00 and 16:30, due to the direction of sunlight and the direction of the roadside unit camera and the weather may affect the light refraction angle changes, resulting in a sharp drop in RVR_1A, between 17:00 and 24:00, the visibility is lowest, below 500, that is, in the case of fog at night, runway sight is lowest.

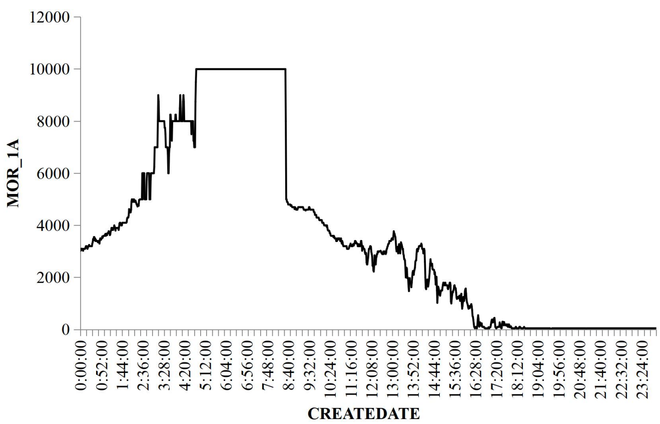

Fig. 7 MOR_1A relative time variation curve.

The best visibility, between 08:30 and 17:30, visibility shows a fluctuating downward trend, from 5000 to 300, between 17:30-24:00, the visibility is the lowest, between 0-300, that is, in the case of fog at night, the meteorological optical range is the lowest. This parameter is consistent with the trend of Figure 6, between 0:00 and 05:00 due to the sky brightness change is gradually from weak to strong process, the change leads to a gradual increase in MOR_1A value, the rest of the change process is consistent with the trend of RVR_1A parameter value.

The Temp (°C) refers to the point at which the air temperature consistently decreases. The DEWPOINT (°C) is the temperature at which water droplets become saturated with air. Fig. 8 illustrates the symmetric relationship between the dew point temperature and the temperature between 0:00 and 12:00, when the temperature was consistently higher than the dew point temperature. The dew point temperature is basically consistent somewhere in the range of 12:00 and 2:00.

Table 1 Airport AMOS observation data field table.

Field	Description	Unit
PAINS HPA	Air pressure	MPa
TEMP	Temperature	℃
RH	Relative humidity	%
DEWPOINT	dew point temperature	℃
RVR_1A	Average RVR value (1 min)	m
MOR_1A	Average MOR value (1 min)	m
WS2A	Average wind speed (2 min)	m/s
WD2A	Average wind direction (2 minutes)	——
CW2A	Average vertical wind speed (2 min)	m/s

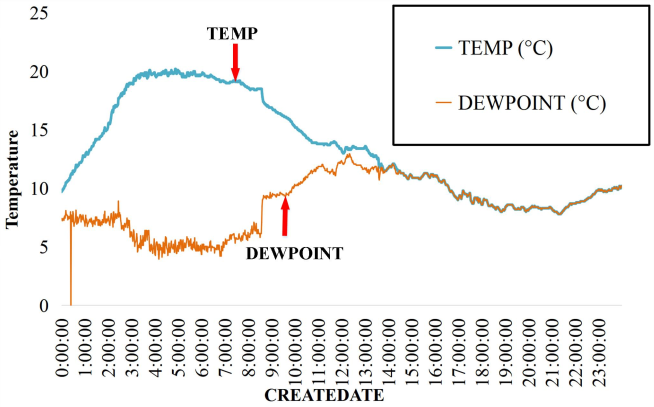

Fig. 8 Relative time variation curves of Temp (℃) and DEWPOINT (℃).

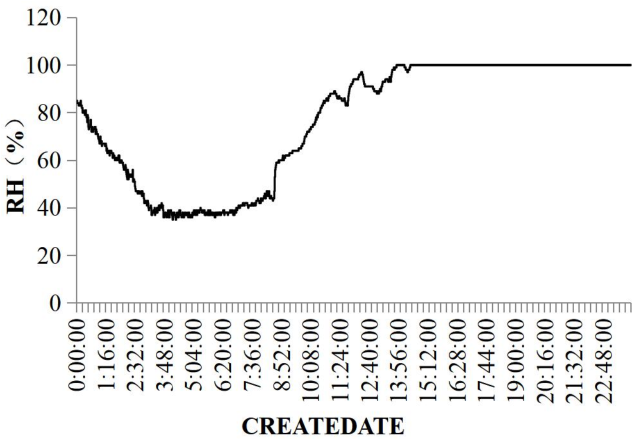

Fig. 9 Relative time variation curve of humidity (RH).

During 0:00-13:40, the relative humidity (RH) first decreased and then increased, and the relative humidity was maintained at 40% during 03:00-08:20, relative humidity was maintained at 100% between 13:40 and 24:00.RH has a certain correlation with TEMP, 0:00-3:40 RH decreases probably because the temperature has warmed up compared to the night, thus causing RH to decrease, and reaches the lowest value of RH at 5:52, after which the water content in the air is larger due to sunlight exposure as well as the continuous rise in temperature, through RH is the percentage of water vapor pressure and saturated water vapor pressure in the air, which can be explained from 6:00-13: 56 RH gradually increases this phenomenon, due to the cooler weather in the second half of the night, the temperature drops, the saturation vapor pressure is low, this time the relative humidity reaches the maximum, the relative humidity value to maintain the maximum value until the moment of temperature rise.

Among them, wind speed affects the concentration of airborne particles through air flow, which leads to changes in visibility, but since the wind speed factor is more complex, we consider the magnitude of the effect of its factor through the Pearson correlation coefficient in the following SPSS data analysis and consider whether to add it to the relevant factors established by the visibility prediction SVR model.

Correlation analysis usually analyzes the correlation between two variables, and its value is between −1 and 1.

Usually, ρ represents the overall correlation coefficient, and the sample correlation coefficient is r .

$$\rho = \frac{\text{cov}(X,Y)}{\sqrt{Var(X)}\sqrt{Var(Y)}} \tag{17}$$

				RVR_1A	TEMP（℃）
RVR_1A	Pearson correlation			1	.765**
	Explicitness (double tail)				.000
	Number of cases			1440	1440
	Self-help sampling [b]	Deviation		0	.000
		Standard error		0	.009
		95 % confidence interval	Lower limit	1	.747
			Upper limit	1	.781

(a) Correlation of RVR_1A—TEMP(℃)

				RVR_1A	RH（%）
RVR_1A	Pearson correlation			1	-.637**
	Explicitness (double tail)				.000
	Number of cases			1440	1440
	Self-help sampling [b]	Deviation		0	.000
		Standard error		0	.012
		95 % confidence interval	Lower limit	1	-.660
			Upper limit	1	-.613

(b) Correlation of RVR_1A—RH(%)

				RVR_1A	CW2A（MPS）
RVR_1A	Pearson correlation			1	.637**
	Explicitness (double tail)				.000
	Number of cases			1440	1440
	Self-help sampling [b]	Deviation		0	.000
		Standard error		0	.013
		95 % confidence interval	Lower limit	1	.614
			Upper limit	1	.662

(c) Correlation of RVR_1A—CW2A

				RVR_1A	WD2A
RVR_1A	Pearson correlation			1	-.532**
	Explicitness (double tail)				.000
	Number of cases			1440	1440
	Self-help sampling [b]	Deviation		0	.000
		Standard error		0	.025
		95 % confidence interval	Lower limit	1	-.581
			Upper limit	1	-.482

(d) Correlation of RVR_1A—WD2A

				RVR_1A	DEWPINT
RVR_1A	Pearson correlation			1	-.110**
	Explicitness (double tail)				.000
	Number of cases			1440	1440
	Self-help sampling [b]	Deviation		0	-.001
		Standard error		0	.019
		95 % confidence interval	Lower limit	1	-.148
			Upper limit	1	-.075

(e) Correlation of RVR_1A—DEWPINT

				RVR_1A	WS2A
RVR_1A	Pearson correlation			1	.614**
	Explicitness (double tail)				.000
	Number of cases			1440	1439
	Self-help sampling [b]	Deviation		0	.000
		Standard error		0	.013
		95 % confidence interval	Lower limit	1	.590
			Upper limit	1	.639

(f) Correlation of RVR_1A—WS2A

				RVR_1A	PAINS
RVR_1A	Pearson correlation			1	-.717**
	Explicitness (double tail)				.000
	Number of cases			1440	1439
	Self-help sampling [b]	Deviation		0	.000
		Standard error		0	.009
		95 % confidence interval	Lower limit	1	-.736
			Upper limit	1	-.698

(g) Correlation of RVR_1A—PAINS

Fig. 10 Correlation analysis between RVR_1A and meteorological factors.

In SPSS programming, we dissected the relationship between runway sight (RVR_1A), meteorological optical sight (MOR_1A), and meteorological variables, as displayed in Figs. 11 and 12.

The Pearson correlation coefficients between RVR_1A and seven meteorological factors, including temperature, relative humidity, station pressure, dew point temperature, 2-minute average wind speed, 2-minute normal breeze heading, and 2-minute normal vertical breeze speed, are 0.76, 0.637, 0.717, 0.110, 0.614, 0.532, and 0.637.

Respectively, as shown in Fig. 10. In accordance with the correlation setting, the absolute value of the correlation coefficient is determined: 0-0.09 indicates no correlation, 0.1-0.3 indicates a weak correlation, 0.3-0.5 indicates a moderate correlation, and 0.5-1.0 indicates a strong correlation. The correlation between dew point temperature and the other variables is 0.110, which is a weak correlation. Excluding this factor, the correlation between the remaining six meteorological factors is strong. Thus, the other six meteorological factors are selected as the influencing factors of RVR_1A.

				MOR_1A	TEMP（℃）
MOR_1A	Pearson correlation			1	.964**
	Explicitness (double tail)				.000
	Number of cases			1440	1440
	Self-help sampling [b]	Deviation		0	.000
		Standard error		0	.002
		95 % confidence interval	Lower limit	1	.950
			Upper limit	1	.957

(a) Correlation of MOR_1A—TEMP(℃)

				MOR_1A	RH（%）
MOR_1A	Pearson correlation			1	-.947**
	Explicitness (double tail)				.000
	Number of cases			1440	1440
	Self-help sampling [b]	Deviation		0	.000
		Standard error		0	.002
		95 % confidence interval	Lower limit	1	-.962
			Upper limit	1	-.943

(b) Correlation of MOR_1A—RH(%)

				MOR_1A	PAINS（HPA）
MOR_1A	Pearson correlation			1	-.845**
	Explicitness (double tail)				.000
	Number of cases			1440	1440
	Self-help sampling [b]	Deviation		0	.000
		Standard error		0	.007
		95 % confidence interval	Lower limit	1	-.857
			Upper limit	1	-.831

(c) Correlation of MOR_1A—PAINS

				MOR_1A	WD2A
MOR_1A	Pearson correlation			1	-.118**
	Explicitness (double tail)				.000
	Number of cases			1440	1440
	Self-help sampling [b]	Deviation		0	.000
		Standard error		0	.023
		95 % confidence interval	Lower limit	1	-.164
			Upper limit	1	-.073

(d) Correlation of MOR_1A—WD2A

				MOR_1A	CW2A
MOR_1A	Pearson correlation			1	.554**
	Explicitness (double tail)				.000
	Number of cases			1440	1440
	Self-help sampling [b]	Deviation		0	.000
		Standard error		0	.018
		95 % confidence interval	Lower limit	1	.520
			Upper limit	1	.588

(e) Correlation of MOR_1A—CW2A

				MOR_1A	DEWPINT
MOR_1A	Pearson correlation			1	-.667**
	Explicitness (double tail)				.000
	Number of cases			1440	1440
	Self-help sampling [b]	Deviation		0	.000
		Standard error		0	.012
		95 % confidence interval	Lower limit	1	-.689
			Upper limit	1	-.641

(f) Correlation of MOR_1A—DEWPINT

				MOR_1A	WS2A
MOR_1A	Pearson correlation			1	.665**
	Explicitness (double tail)				.000
	Number of cases			1439	1439
	Self-help sampling [b]	Deviation		0	.000
		Standard error		0	.013
		95 % confidence interval	Lower limit	1	-.638
			Upper limit	1	-.691

(g) Correlation of MOR_1A—WS2A

Fig. 11 Correlation analysis between MOR_1A and meteorological factors.

The Pearson correlation coefficients between MOR_1A and seven meteorological variables, including temperature, relative humidity, station pressure, dew point temperature, 2-minute average wind speed, 2-minute average wind direction, and 2-minute average vertical wind speed, are 0.964, 0.947, 0.845, 0.667, 0.665, 0.118, and 0.554, respectively, as shown in Fig. 11. The correlation of the average 2-minute wind direction is 0.118, which is a weak correlation. Therefore, excluding this factor, the correlation of the other six meteorological factors is a strong correlation. Thus, the other six meteorological factors are selected as the influencing factors of MOR_1A.

V. EXPERIMENT AND RESULT ANALYSIS

A. MOR DATA PREPROCESSING

According to the data processing in section 4, we can obtain the relationship between meteorological variables and visibility in fog video data, which lays the foundation for establishing a visibility deep learning model. The frames of video data obtained by the road test unit are then preprocessed. First, the unobstructed path line in the area of interest is aligned to determine the start and end points of the path line, and the direction position of the start and end points is recorded. There are public guidelines for the length, width, and spacing of path lines on highways. Inquiring about the national expressway lane line standard reveals that the lane line consists of 69 lines, the white line is 6 meters long, the interval is 9 meters, and the cycle is 15 meters. Therefore, the actual length of the white line at the starting point for calibration is 6 meters. The following figure shows:

Fig. 12 Lane line image calibration.

Secondly, the dark channel diagram of the experimental model is obtained by MATLAB:

Fig. 13 Acquisition of dark channel graph.

Fig. 14 Diagram of dark channel and transmittance

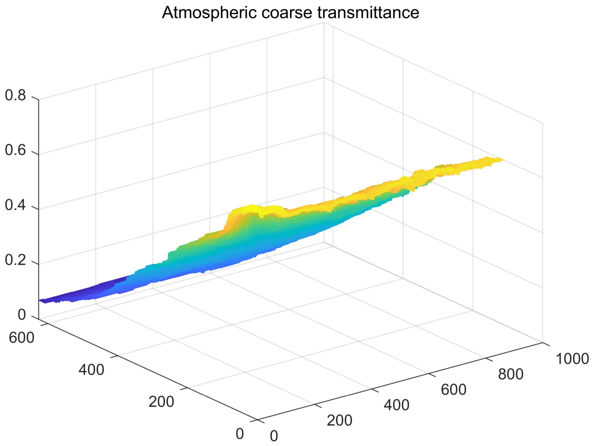

Fig. 15 Acquisition map of coarse atmospheric transmittance.

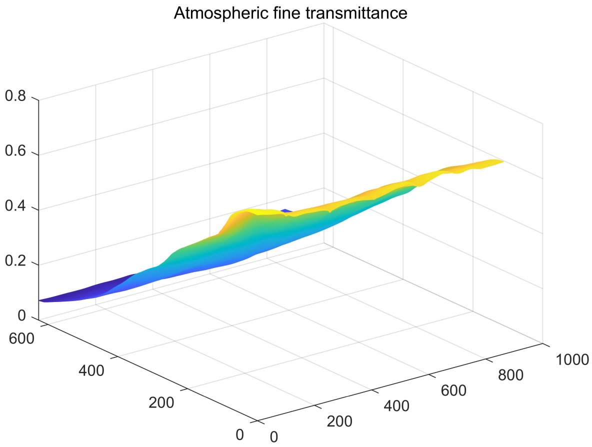

Fig. 16 Refined transmittance acquisition.

The dark channel graph deals with the region of interest obtained in the previous step. Then, we must obtain the transmittance to proceed with the visibility calculation. According to the transmittance calculation formula (5), the atmospheric brightness is unknown, and the transmittance can be determined by using the conventional dark channel method to calculate 0.1 percent of the pixels with brightness values at the front of the dark channel image. To create the atmospheric coarse coefficient map, the most expensive component cost is applied to the appropriate pixels within the stock Fig. 14.

The above chart reveals that the large fluctuations in atmospheric transmittance are a result of the instability of visible light.To accurately calculate the visibility value, the atmospheric transmittance must be refined. We use MATLAB algorithm based on guided filtering to obtain the refined transmittance.

According to Formulas (6)-(10), the MOR value in this period can be calculated. As shown in Fig. 17, we output the identified visibility, calculate the visibility of each frame, incorporate the parameters into the algorithm, and plot the time-dependent visibility curve.

In this paper, five-fold cross-validation $(5\text{-}CV)$ is used to obtain the accuracy of the model. According to Formula (16), in order to predict the MOR value at time t, we require the MOR value at the first n moments of time t, where n is the step size. In this study, the step size n is eight, or the MOR value at the first eight moments of each input, in order to predict the MOR value at the current time t. As shown in Fig. 18, the prediction model is established based on the established SVR architecture.

Finally, we fit the existing MOR data based on the SVR prediction model diagram. The fitting effect diagram is shown in Fig. 18. The actual value of the meteorological optical range detected by the test is essentially consistent with the data change trend of the training value, and the error value falls within the range of [-0.7, -2.0]. Because the algorithm must calculate and validate the training data, the training data lags behind the actual data. The figure indicates that the lag time is between 0.9 and 1.1 seconds, but the meteorological optical range data calculated by the SVR model is smoother than the actual data, which is consistent with the results of the actual data monitoring.

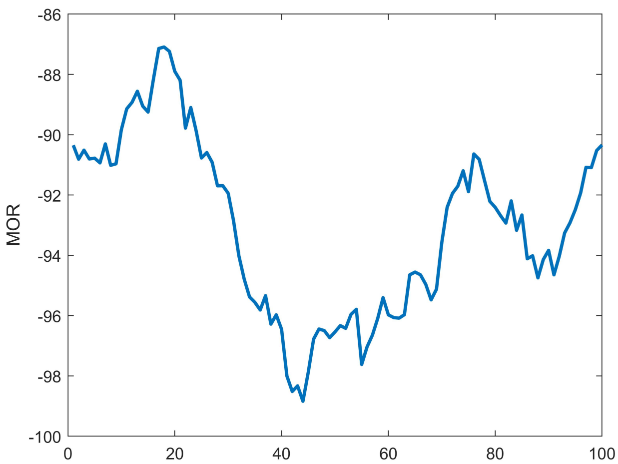

Fig. 17 Visibility chart.

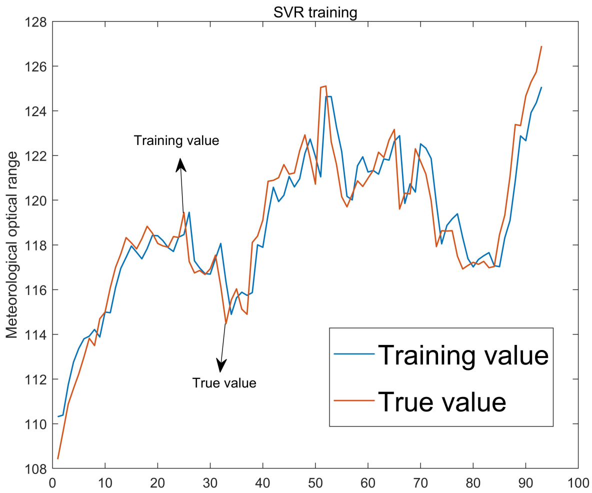

Fig. 18 Rendering of MOR data comparison.

B. MOR DATA PREDICTION

The 2~36 minute image gradient was calculated using Sobel, Roberts, and Prewitt, but did not match visibility well. Figs. 19-22 use Sobel, Roberts, and Prewitt gradient functions to obtain image gradients to determine image clarity.

The depth learning model of visibility estimation based on video data is then used to compare the obtained clarity with the estimated visibility based on video data, and a comparison is obtained.

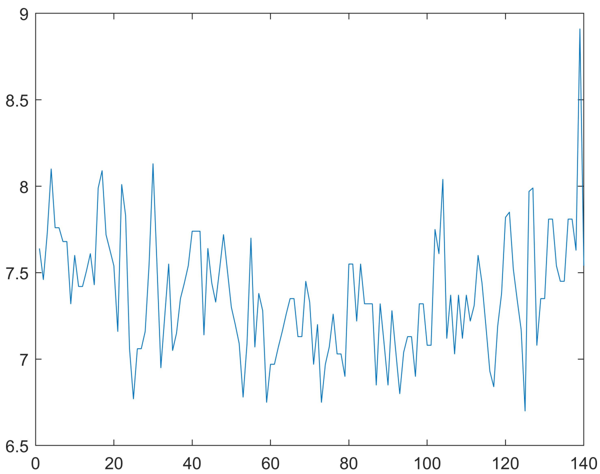

Fig. 19 Image visibility detection.

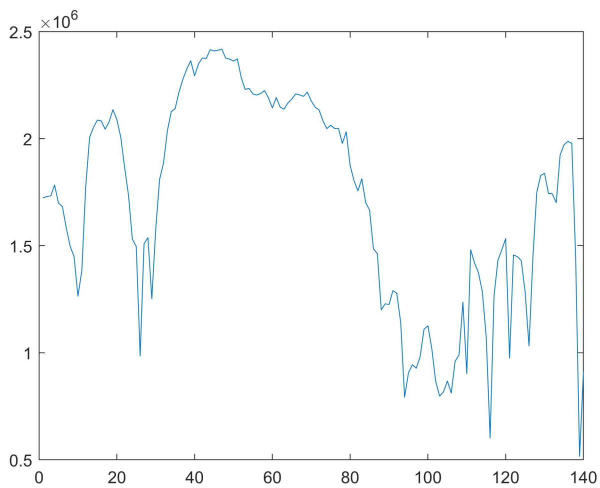

Fig. 20 Image gradient of Sobel algorithm.

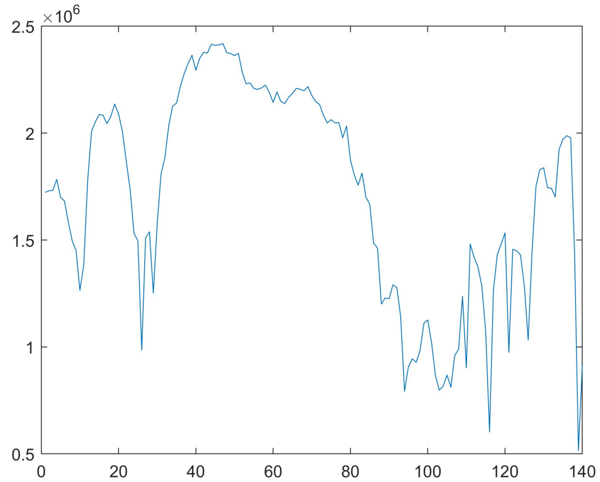

Fig. 21 Roberts algorithm image gradient.

As can be seen from Figure 24, comparing the change curves of visibility MOR values after Sobel, Roberts, and Prewitt gradient image transformations, the Prewitt edge detection method is less robust for the detection of noisy images and fine edge images, and does not consider the influence of the distance of neighboring points on the current pixel point, which will lead to poorer detection results, the curve matches the predicted visibility curve change rate. The area calculation method is used if both the unit and the rate of change are consistent. According to the visibility prediction model in this paper, the estimated visibility accuracy rate is 80.29%. Fig. 25 depicts the MOR value of the future fog change trend, as predicted by the established model of prediction.

From Fig. 25, it is clear that the highway meteorological optical visible range gradually increased, and the fog gradually dissipated, especially in the next 15 to 28 minutes at the fastest rate of dissipation, after the 45th minute to peak, and maintained the visible range value until the end of the forecast stage, in accordance with the 'Road Traffic Safety Law of the People's Republic of China Implementation Regulations' highway visible range of fewer than 50 meters from the nearest exit as soon as possible from the highway, the weather conditions are not suitable for highway travel. This paper establishes the meteorological optical visible range of 152 meters or more for normal travel, i.e., the experimental results for the analysis of the vehicle's ability to travel normally after 25 minutes.

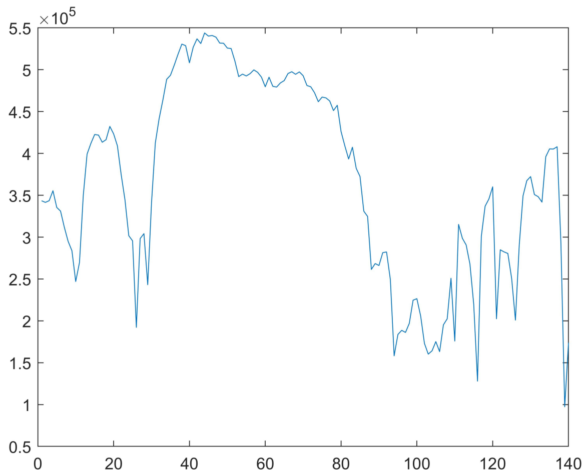

Fig. 22 Prewitt algorithm image gradient.

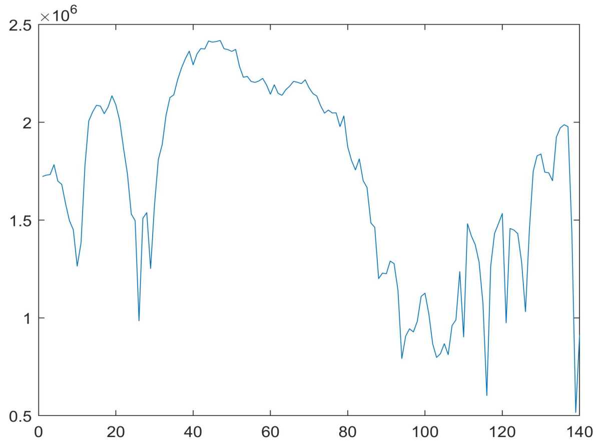

Fig. 24 Visibility and clarity comparison chart based on video data.

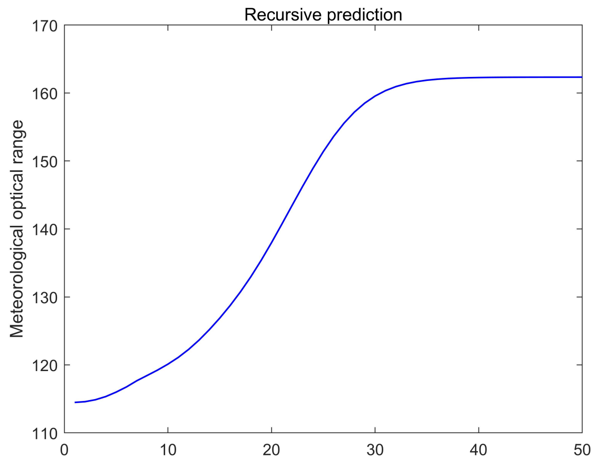

Fig. 25 MOR Recursive Prediction Graph.

C. COMPARATIVE EXPERIMENT AND ANALYSIS

On the highway data set, the proposed algorithm is compared to the visibility detection algorithms based on convolutional neural network and BP neural network in a comparative experiment. First, the visibility prediction values for the subsequent period are obtained using three different techniques, as depicted in Table 2.

The method for calculating its accuracy is defined as detection results within the range [actual value -0.8, actual value +0.8] that are recorded as accurate data，where A_i denotes the number of data with predicted values other than [actual value -0.8, actual value +0.8], B_i denotes the data with predicted values in [actual value -0.8, actual value +0.8], and C_i denotes the total number of data. The number of accurate data for the three methods is shown in Table 3-5.

The accuracy of each method can be found according to the accuracy calculation formula $T = \frac{A_i}{C_i}$. Calculations are performed to compare the test accuracy of the three algorithms on the highway dataset, as shown in Table 6.

First, we conduct tests and comparisons on the highway data set, whose category distribution is well-balanced. This paper compares the performance of the three algorithms on this data set according to the accuracy index. Table 2 demonstrates that a variety of algorithm models have produced good results on the highway data set, with the SVR visibility prediction method proposed in this paper achieving the highest level of accuracy (84.21%). Second, because the method presented in this paper simplifies the visibility prediction model, the detection speed is faster than with BP neural network and convolutional neural network visibility prediction methods. Due to the small sample size of the extracted comparative reference data, the accuracy will be low; however, the accuracy of the three visibility prediction methods exceeds 70%. In addition, the low accuracy rate may be due to the fact that the highway data set consists of a single road area scene map. On the highway, the image contains only relatively monotonous targets, such as guardrails and pavements, and there are few significant feature details available. The image belongs to the perspective of overlooking observation, image similarity between similar categories is high, and the image's shooting perspective is also different. The fog environment in the real scene is more complex than the synthetic fog. Visibility detection in highway images is evidently more complex and challenging.

Table 2 Visibility prediction test data table

Method / Time h	BP neural network	SVR	Convolutional neural network	Actual value
5	113.0	113.2	114.1	111.1
10	114.5	114.0	114.3	113.7
15	117.0	114.8	115.7	116.6
20	118.5	118.0	118.1	117.8
25	117.6	117.0	117.3	117.0
30	114.9	115.6	114.9	117.1
35	115.0	115.1	115.0	115.8
40	118.1	118.2	118.0	118.7
45	121.4	121.3	121.6	121.0
50	122.2	122.8	121.9	120.5
55	119.9	121.0	120.8	121.3
60	120.2	120.3	120.1	120.9
65	119.2	119.7	119.3	120.0
70	121.7	121.5	121.9	120.8
75	118.7	118.3	118.2	118.3
80	117.3	117.1	117.2	117.2
85	116.9	116.7	116.8	116.7
90	122.7	122.8	123.9	123.2
95	124.6	125.0	124.4	125.7

Table 3 BP Neural Network Visibility Prediction Model Detection Results Table

Algorithm	A_i	B_i
BP neural network	4	15

Table 4 Convolutional Neural Network Visibility Prediction Model Detection Results Table

Algorithm	A_i	B_i
Convolutional neural network	5	14

Table 5 SVR visibility prediction model test results table

Algorithm	A_i	B_i
SVR	3	16

Table 6 Visibility test accuracy and speed comparison table

Algorithm	Accuracy (%)	Operating speed (s)
BP neural network	78.94	18.7
Convolutional neural network	73.68	15.2
SVR	84.21	10.7

Table 7 Table of visibility prediction results based on SVR visibility prediction model, convolutional neural network and BP neural network after increasing the number of samples

Algorithm	A_i	B_i
SVR	210	2790
Convolutional neural network	366	2634
BP neural network	432	2568

In order to solve the problem of small data samples, a large number of sample sets were added in the subsequent experiments, and the visibility prediction results are shown in Table 7.

By adding a large number of samples to observe the visibility detection accuracy of the three methods, it is calculated that the visibility detection accuracy based on SVR reaches 93%, the visibility prediction accuracy based on convolutional neural network is 87.7%, and the visibility prediction accuracy based on BP neural network is 85.6%, which is due to the fusion of the proposed method in this paper considering visibility influencing factors in many aspects The dark channel method and refinement of light transmission rate, comparing various edge processing methods, selecting the processing method with better marginalization to delineate the visibility detection area, and finally conducting visibility detection according to the SVR visibility prediction model to achieve accurate visibility prediction.

VI. Conclusion

In this paper, a road visibility prediction model suitable for fog environment is established through the functional relationship between visibility and meteorological variables. The model reduces the complexity of the algorithm and improves the efficiency of data processing. The problem of inaccurate calculation of light transmission rate under fog conditions is solved, and the exact duration of fog dissipation is accurately predicted. Finally, 5-fold cross-validation was used to determine the accuracy of the model. The visibility prediction method based on the fusion of improved dark channel and SVR model was validated by conducting experimental tests based on the obtained real highway visibility detection video data. In the actual test, convolutional neural network and BP neural network models were also used for visibility prediction, and the advantages and disadvantages of the visibility prediction method based on the fusion of improved dark channel and SVR model were demonstrated by comparing the 19 sets of visibility values predicted by each method with the real values, where the experiments were evaluated by the accuracy of visibility prediction and the time spent on predicting visibility. The calculation results show that the method proposed in this paper can effectively solve the problem of large errors in the predicted visibility values by establishing an SVR visibility prediction model suitable for visibility prediction through multi-factor analysis and refining the light transmission rate, and finally analyzing the reasons for the high accuracy of the method. The experimental results show that the method can improve the speed of visibility prediction and greatly improve the detection accuracy. Compared with the visibility prediction method based on GA-BP neural network model, the detection speed is improved by 15.8% and the accuracy is increased by 1%. Finally, by adding a large number of data samples, the accuracy of the SVR visibility-based prediction model can reach 93%.

The method proposed in this paper solves the problem of low accuracy of visibility detection caused by weather, the method has high prediction accuracy, which is important to improve the safety of driving vehicles in extreme weather, and provides a technical basis for our team's subsequent pseudo-obstacle detection in extreme conditions, and the coming research will focus on pseudo-obstacle detection in extreme conditions.

References

[1] Xue D, Liu Q. Relationship between Air Pollutants and Visibility in Shanghai during 2006-2010[C]//Applied Mechanics and Materials. Trans Tech Publications Ltd, 2014, 675: 314-317.

[2] Zhou B, Du J, Gultepe I, et al. Forecast of low visibility and fog from NCEP: Current status and efforts[J]. Pure and applied geophysics, 2012, 169(5): 895-909.

[3] Castillo-Botón C, Casillas-Pérez D, Casanova-Mateo C, et al. Machine learning regression and classification methods for fog events prediction[J]. Atmospheric Research, 2022, 272: 106157.

[4] Cornejo-Bueno S, Casillas-Pérez D, Cornejo-Bueno L, et al. Statistical analysis and machine learning prediction of fog-caused low-visibility events at A-8 motor-road in Spain[J]. Atmosphere, 2021, 12(6): 679.

[5] Arun S H, Singh C, John S, et al. A study to improve the fog/visibility forecast at IGI Airport, New Delhi during the winter season 2020–2021[J]. Journal of Earth System Science, 2022, 131(2): 1-11.

[6] Saadatseresht M, Varshosaz M. Visibility prediction based on artificial neural networks used in automatic network design[J]. The Photogrammetric Record, 2007, 22(120): 336-355.

[7] Guijo-Rubio D, Gutiérrez P A, Casanova-Mateo C, et al. Prediction of low-visibility events due to fog using ordinal classification[J]. Atmospheric Research, 2018, 214: 64-73.

[8] Liaw J J, Chen K Y. Using High-Frequency Information and RH to Estimate AQI Based on SVR[J]. Sensors, 2021, 21(11): 3630.

[9] Won W S, Oh R, Lee W, et al. Hygroscopic properties of particulate matter and effects of their interactions with weather on visibility[J]. Scientific reports, 2021, 11(1): 1-12.

[10] Ashrit R. Assessment of forecast skill of high-and coarse-resolution numerical weather prediction models in predicting visibility/fog over Delhi, India[J]. Current Science (00113891), 2021, 120(4).

[11] Sakaridis C, Dai D, Van Gool L. Semantic foggy scene understanding with synthetic data[J]. International Journal of Computer Vision, 2018, 126(9): 973-992.

[12] Ren X, Li X, Ren K, et al. Deep learning-based weather prediction: a survey[J]. Big Data Research, 2021, 23: 100178.

[13] Yan S, Zheng Y, Chen Y, et al. Atmospheric visibility prediction based on multi-model fusion[C]//2021 International Conference on Image, Video Processing, and Artificial Intelligence. SPIE, 2021, 12076: 168-175.

[14] Zhang Y, Wang Y, Zhu Y, et al. Visibility Prediction Based on Machine Learning Algorithms[J]. Atmosphere, 2022, 13(7): 1125.

[15] Han J H, Kim K J, Joo H S, et al. Sea Fog Dissipation Prediction in Incheon Port and Haeundae Beach Using Machine Learning and Deep Learning[J]. Sensors, 2021, 21(15): 5232.
[16] Tao H C, Li X H, Zhang Z B, et al. Estimation and prediction of fog day-based visibility based on convolutional neural network[C]//International Conference on Image Processing and Intelligent Control (IPIC 2021). SPIE, 2021, 11928: 56-64.
[17] Tang P, Song S, Zhao T, et al. Visibility estimation of foggy weather based on continuous video information[J]. Remote Sensing Letters, 2021, 12(10): 1061-1072.
[18] Nayar S K, Narasimhan S G. Vision in bad weather[C]//Proceedings of the seventh IEEE international conference on computer vision. IEEE, 1999, 2: 820-827.
[19] Tan R T. Visibility in bad weather from a single image[C]//2008 IEEE conference on computer vision and pattern recognition. IEEE, 2008: 1-8.
[20] Kim B Y, Cha J W, Chang K H, et al. Visibility Prediction over South Korea Based on Random Forest[J]. Atmosphere, 2021, 12(5): 552.
[21] Iqbal M, Riaz M M, Ghafoor A, et al. Guided image filtering using data mining and decomposition[J]. The Imaging Science Journal, 2019, 67(5): 261-267.
[22] Wagh S, Kulkarni R, Lonkar P, et al. Development of visibility equation based on fog microphysical observations and its verification using the WRF model[J]. Modeling Earth Systems and Environment, 2022: 1-17.
[23] Riyadh Rahef Nuiaa, Selvakumar Manickam, Ali Hakem Alsaeedi, and Esraa Saleh Alomari, "Enhancing the Performance of Detect DRDoS DNS Attacks Based on the Machine Learning and Proactive Feature Selection (PFS) Model," IAENG International Journal of Computer Science, vol. 49, no.2, pp511-524, 2022.
[24] Fatima Zahra Fagroud, Hicham Toumi, El Habib Ben Lahmar, Khadija Achtaich, Sanaa El Filali, and Youssef Baddi, "Connected Devices Classification using Feature Selection with Machine Learning," IAENG International Journal of Computer Science, vol. 49, no.2, pp445-452, 2022
[25] Emanuel A W R, Paulus M, Nugraha J A M. Snapshot-based human action recognition using OpenPose and deep learning[J]. Snapshot-Based Human Action Recognition using OpenPose and Deep Learning, 2021, 48(4): 2-8.
[26] Wu J, Zhang J, Nie B, et al. Adaptive control of PMSM servo system for steering-by-wire system with disturbances observation[J]. IEEE Transactions on Transportation Electrification, 2021, 8(2): 2015-2028.
[27] Wu J, Kong Q, Yang K, et al. Research on the steering torque control for intelligent vehicles co-driving with the penalty factor of human-machine intervention[J]. IEEE Transactions on Systems, Man, and Cybernetics: Systems, 2022.
[28] Wu J, Zhang J, Tian Y, et al. A novel adaptive steering torque control approach for human–machine cooperation autonomous vehicles[J]. IEEE Transactions on Transportation Electrification, 2021, 7(4): 2516-2529.
[29] Wu J, Tian Y, Walker P, et al. Attenuation reference model based adaptive speed control tactic for automatic steering system[J]. Mechanical Systems and Signal Processing, 2021, 156: 107631.